Indoor Pedestrian Localisation Solution based on Anemometry Sensor Integration with a Smartphone

Guillaume Trehard, Mehdi Boukallel and Sylvie Lamy-Perbal

CEA, LIST, Sensorial and Ambiant Interfaces Laboratory
91191 - Gif-sur-Yvette CEDEX, FRANCE

***Abstract*—The paper deals with the design, calibration and experimental validation of a novel infrastructure-less solution dedicated to indoor pedestrian localisation issues. The approach involves aerodynamic fluid computation for instantaneous speed estimation of a pedestrian handling a smartphone. For this purpose, a differential pressure-based MEMS anemometer is integrated to an Android smartphone by means of a dedicated PIC 32 bits microcontroller. Measurements of the pedestrian orientation are ensured by a gyroscope sensor coupled with the smartphone. Consequently, both instantaneous speed and heading measurements are combined to the dead reckoning technique for estimating the 2D relative position of the user. Theoretical modeling is conducted in order to calibrate and quantify the accuracy of the sensor. In *situ* experiments along straight paths demonstrate that the sensors coupled with a smartphone achieve pedestrian localisation with average accuracy of less than 6 % of the total travelled distance.**

***Index Terms*—Indoor pedestrian localisation, infrastructure-less solution, sensor augmented smartphone, localisation based service, smart sensors.**

I. INTRODUCTION

During the last decade, we are experiencing an increasing interest for indoor pedestrian localisation services. In fact, the rapid growth of Localisation Based Services (LBS) is motivated on the one hand by the recent technological progress involved in smartphones design and on the other hand by the added value provided by LBS for urban mobility. The LBS use commonly the location of nomadic devices to deliver appropriate services to the user. Thus, the accurate determination of the user localisation is the key features of an efficient technological solution. Ultimately, indoor localisation-based technologies have to be ubiquitous, fading into the background, cost effective and naturally supported by all nomadic devices.

According to literature, the indoor pedestrian localisation has been initially addressed by pre-installed infrastructure solutions (GNSS, UWB, WIFI, Cell Id, RFID,...) [1] [2] [3] [4] [5]. Even if these solutions are smartphone oriented with sub-meter accuracies, they require large amounts of infrastructure to be installed into the environment or an extended and reliable calibration process to ensure accurate location determination. The cost and constraints introduced by those approaches may limit the frame of usability to specific applications.

In the light of those observations, recent research efforts have been put in the development of infrastructure-less solutions based on range of technological solutions including inertial, camera and magnetometry techniques. From first results stressed by the literature [6] [7], infrastructure-less solutions can achieve indoor localisation with a meter accuracy. A common solution consists in equipping the user or the smartphone with additional sensors in conjunction to dedicated computation resources in order to catch the dynamics of walking experienced by the pedestrian. Even if encouraging results are presented, developed solutions remain computationally expensive and suffer from the lack of scalability limiting the scope for applications involving mobility.

In fact, vision-based solutions achieve localisation with a standard deviation of about $\pm$ 1 to 2 m but require real-time computing resources for constant performances. Li *et al.* [8], introduced recently an original vision-based positioning method with the use of single camera and newly defined 3D map for indoor localisation and navigation issues. The positioning procedure is performed in two phases: image processing and pose estimation. In the image processing phase, images grabbed in real time are matched with the 3D map (collection of geo-referenced images) to recognize and identify feature points in the environment using a dedicated algorithm.

Magnetic based-approach offers the opportunity to achieve a smart integration with the smartphone [9] due to the compact size of available sensors nowadays. However, the accuracy of localisation is sensitive to the magnetic response of the environment in the vicinity of the user. Consequently, large magnetic deviations can be observed leading to an unprecise localisation. The first system based on the above solution can be attributed to Foxlin [10]. Foxlin's system uses a tri-axial magnetometer sensor to compute a yaw measurement that is used as an input measurement to feed an Indirect Kalman Filter (IKF). Experimental results showed a good performance in a wood-frame house. However, a limitation is that magnetometers are unusable in steel structure and many other indoor environments [11]. Moreover, this technique is commonly related to a fingerprinting-based approach and requires to perform the magnetic mapping of the environment.

978-1-4673-1954-6/12/$31.00

Comparing to existing infrastructure-less techniques, the Inertial Navigation System (INS) approach has been extensively studied the last years due to the outstanding localisation accuracy which could be achieved [9] [12] [13]. In its most common implementation, the state-of-the-art solution consists of a small 6-DOF MEMS Inertial Measurement Unit (IMU) providing rate-of-rotation and acceleration measurements. These measurements are used in a strapdown inertial computer to estimate the pedestrian's location according to a known starting position. Nevertheless, IMU suffers usually from important drift errors and requires expensive computational resources for real-time error compensation (Kalman filtering, Bayesian approach ...). [14] [15] [16].

We propose to address, in this paper, the issue of indoor pedestrian localisation based on a infrastructure-less solution by a novel technological approach aiming to bring new solutions to this field. It consists of a smartphone augmented sensors with hybridization approach involving anemometer and gyroscopic sensors. In fact, a differential pressure-based MEMS anemometer is integrated to an Android smartphone by means of a dedicated Microchip PIC 32 bits microcontroller. Hence, the instantaneous pedestrian velocity along the walking direction is measured according to air flow dynamics experienced by the anemometer. Since drift errors are reduced with the MEMS anemometer, speed signals could be easily computationally manipulated for estimating the walking distance, without the need of the step length as required in podometry techniques.
As a matter of fact the anemometer delivers measurements along the walking heading, achieving 2D pedestrian localisation requires orientation measurements. Consequently, sensor fusion technique is implemented between the anemometer and the gyroscope (IDG300 dual-axis from InvenSens). Dedicated computational algorithm has been developed in the PIC 32 platform in order to ensure signal processing, sensor fusion and position estimation. Extensive indoor experiments have been conducted in order to validate the efficiency and the robustness of the adopted approach.

The paper is organized as follows. The foundations of the anemometry approach are given in section II. In the section III, details on the sensor calibration and the accuracy determination are provided for both static and dynamic cases. Section IV presents the designed prototype and experimental results issued from trials. Finally, section V concludes the paper and introduces future works under development.

II. ANEMOMETRY APPROACH

The aim of the designed system is to perform indoor pedestrian localisation based on measuring the user (pedestrian) velocity. This latter can be addressed by determining the air flow velocity produced by the user in the environment. This technique is well adapted to indoor configurations where draught is commonly limited or controlled (buildings, museum ...).

According to the literature, the air flow velocity can be measured by various methods, commonly referring to anemometry, using a broad physical principles. Among different existing techniques, only few anemometers fit requirements of the pedestrian dynamics (eg. sensitivity, accuracy). Three main approaches appeared relevant to case study involved in the paper: ultrasound anemometer, hot-wire anemometer or pressure-based anemometer. After a benchmark of selected solutions based on criteria such as the sensitivity, the robustness and the cost, we focused on the third technique and especially on the Pitot tube theory. This approach is indeed widely used and could be adapted to the case of study.

A. Pitot tube theory

The Pitot tube theory is an application of Bernoulli's equation for measuring the velocity of a fluid in the flow direction. Assuming that the altitude is constant and considering only positive speeds in the flow direction, a Pitot tube sensor would be ruled by equation (1).

$$V_{fluid} = \sqrt{2 \times \frac{p_t - p_s}{\rho}} \tag{1}$$

where V_{fluid} is the fluid velocity, p_t the total pressure, p_s the static pressure and ρ the fluid density (which is, in our case, the air density).

If the measurement $\Delta p = p_t - p_s$ is known, and assuming that the pedestrian walking velocity is smaller than air density variations, equation (1) can be simplified to:

$$V_{fluid} = Constant \times \sqrt{\Delta p} \tag{2}$$

where the constant may be determined according to an experimental calibration procedure.

B. Sensor specifications according to air flow dynamics

The main assumption presented is that draught is commonly limited or controlled in our case application. The assumption is obviously arguable and could restrict the field of application. However, it appears that this hypothesis is mostly acceptable in the pedestrian indoor localisation context. Therefore, we can consider that $V_{fluid} = V$ where V is the pedestrian velocity. It is worth noting that air stream effects are minor except for important air flow variation. This issue will be discussed in section IV-D.
The range and the resolution required for a Pitot tube with a differential pressure sensor need to be specified. Using the same hypothesis than in II-A, the Bernoulli's equation (1) can also be written:

$$\Delta p = \frac{1}{2}\rho V^2 \tag{3}$$

Robin *et al.* have developed a discrete modeling of human walking behavior [17] in which they measured and classified several pedestrian walks. The paper underlines that velocity range for pedestrian is comprised between 0.5 m/s and 2.5 m/s, with an average around 1.3 m/s. Taking into consideration those averaged speeds and adding margins, we assume that the pedestrian walk is comprised between 0 m/s and 5 m/s. Additionally, the air density is approximated to 1.2 kg/m^3 (value at sea level and 20°C). Those assumptions and equation (3) consequently lead to write:

$$0Pa \leq \Delta p \leq 15Pa$$

Moreover, in order to achieve the best resolution on this range, we define an acceptable resolution of the system as 0.1 Pa.

C. Sensor selection

A solution of interest fitting the previous requirements (see II-B) is based on thermal micro-flow measurement. For this purpose, a commercial thermal micro-flow MEMS is adopted. In this solution, a constrained air flow is heated and two thermal resistors measure the air flow temperature variation (see figure 1). The temperature gradient is linked to the velocity of the flow.

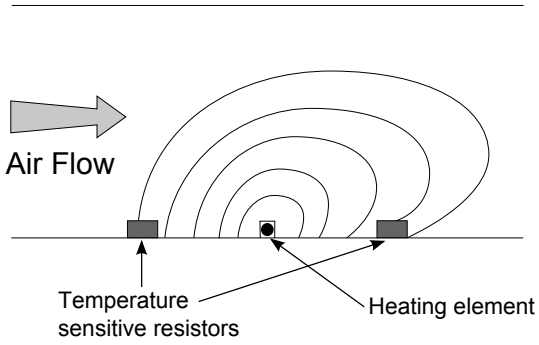

Fig. 1. Principle of the thermal micro-flow measurement

Among available commercial sensors, we selected the LBA series sensor (figure 2) from SensorTechnics GmbH company in view of the outstanding features achieved by the sensor (sensitivity, temperature compensated, cost-effective).

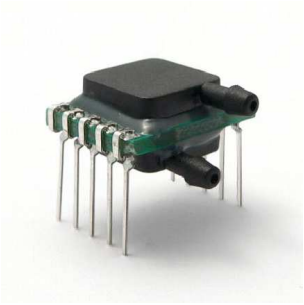

Fig. 2. MEMS thermal micro-flow LBA series sensor from SensorTechnics GmbH

III. SENSOR CALIBRATION AND ACCURACY DETERMINATION

Since the LBA sensor is based on a linear differential pressure principle whereas we aim to measure the air flow velocity, it is crucial to perform both sensor calibration and characterization in order to validate the compatibility of such sensor with the air flow velocity measurement.

A. Sensor calibration

As stated before, the LBA sensor is calibrated to deliver a linear voltage output according to a differential pressure input. If U_s is the sensor output and α, β are constants, the output can be expressed as:

$$U_s = \alpha.\Delta p + \beta \tag{4}$$

Combining this equation with the Pitot tube theory (eq. 2), the velocity of the air flow V can be written:

$$V = sign\sqrt{aU_s + b} \tag{5}$$

where a and b are constants determined by calibration. In our configuration, we have limited measurements to positive speeds, thus $sign$ = 1. In order to perform the sensor calibration, the LBA sensor was introduced in a wind tunnel and the output voltage U_s was measured according to incremental air flow velocities (from 0.25 m/s to 2.7 m/s). The sensor output characteristic according to the air speed is depicted in figure 3 showing obviously the square root shape. From the experimental measurements, a linear regression allows the determination of constants a and b.

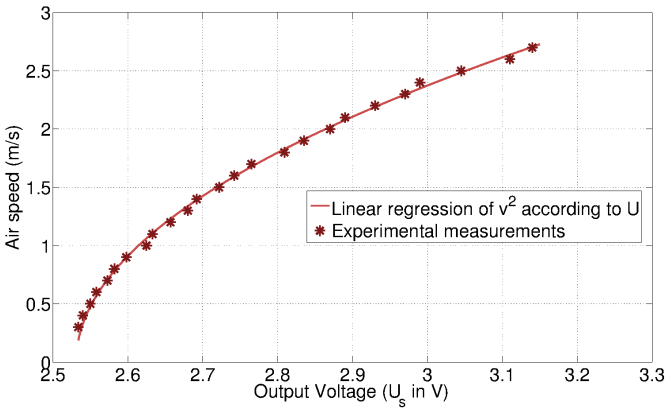

Fig. 3. Measured output characteristic of the LBA sensor

B. Transient response of the sensor

During a walking process at a constant average speed, the pedestrian's velocity signal shape is commonly periodic. Indeed, each period relies to the foot step phase. As mentioned in I, the pedestrian velocity will be numerically integrated to calculate the travelled distance. Therefore, studying the transient response of LBA sensor is required to avoid unprecise

data analysis. This study is achieved by measuring the step response of the sensor to five input magnitudes. Experiments have been conducted in controlled environment (wind tunnel). Figure 4 shows the sensor output signal and table I the time constant for each experimentation.

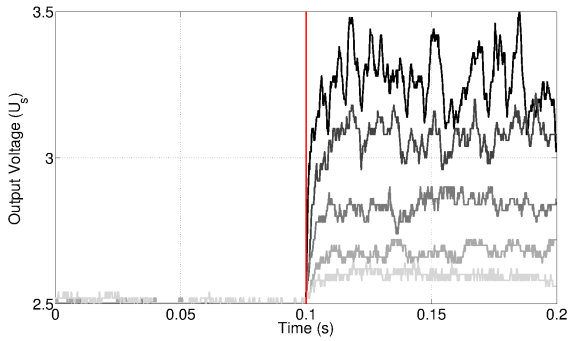

Fig. 4. Transient responses of LBA sensor to step inputs

ΔV (m/s)	2.5	2.0	1.5	1.0	0.5
τ (ms)	1.7	4.2	4.7	5.6	5.6

TABLE I
RESPONSE TIME OF THE LBA SENSOR

As we suspected (eq. 5), the sensor output is not linear. However, the plots can be modeled as a first order system response. Thus, we consider the time constant to be the abscissa of the intersection between the tangent to the origin and the established value of the transient response. These results suggest that the time constant τ of the sensor is less than 10 ms whatever the amplitude of the input signal is. Therefore, we can consider that the sensor is convenient for walks up to 100 Hz frequency which referring to a hundred steps per seconds.

C. Sensor accuracy

Another issue to consider is the accuracy of the sensor for air flow velocity measurements. In fact, at a very low speed (less than 1 m/s), the output voltage U_s from the LBA is around the millivolts and due to the square root shape of the characteristic, the voltage measurement can be complex.
Considering the data sheet of the sensor, the table II gives the total accuracy referring to the combined error due to linearity, pressure hysteresis, offset, span calibration and temperature effects.

Characteristics		Min.	Typ.	Max.	Unit
Non-linearity			±(1.8 % of reading + 0.2 %FSS)	±(2.4 % of reading + 0.3 %FSS)	
Zero pressure offset		2.47	2.50	2.53	V
Full scale span		3.92	4.00	4.02	
Thermal effects	Offset 5...55 °C			±25	mV
	Span 5...55 °C			±2	%FSS
Total accuracy	5...55 °C			±(2.25 % of reading + 2.25 %FSS)	

TABLE II
PART OF THE DATA SHEET OF THE LBA SENSOR

Figure 5 illustrates the maximum effect of the total accuracy on the measured air velocity. In the range between 0.5 m/s and 1.5 m/s, the inaccuracy is important partly due to the square root characteristic of the sensor. As an illustration of this effect, if the pedestrian remains in static configuration (not moving), the measured velocity can be up to 1 m/s mainly due to the total inaccuracy. If the pedestrian is walking at an average speed of 1 m/s, errors could lead the sensor to measure from 0 m/s up to 1.4 m/s with a consequence as inaccuracy in the user position estimation.

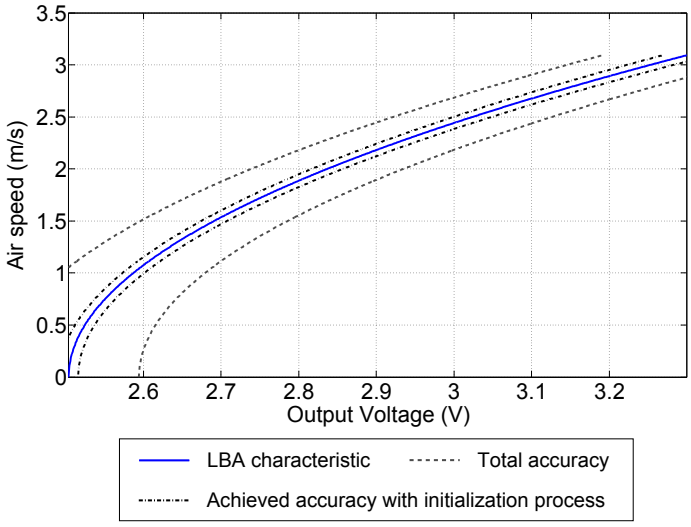

Fig. 5. Inaccuracy effect on the LBA characteristic

It is worth noting that most of the total inaccuracy is due to offsets. Indeed calibration, zero pressure value and temperature affect the sensor output with offsets. For the duration of the experiment, those parameters are assumed to be constant. In fact, from experiments we conducted, we have noticed that the zero pressure offset can be different at each new trial but remains the same during the whole walk. The temperature is assumed to be constant in the indoor configuration (or without important variation). Finally, the sensor characterization performed during the calibration process and ruled by equation 5 exhibits small drifts and remains nearly the same from experiment to experiment

(constants a and b are unchanged).

The overall inaccuracy will be approximated by an offset U_0 which is not varying during the pedestrian walk. This offset can be estimated by a short initialization process before the departure. Therefore, the sensor characteristic (eq. 5) will be adapted to compensate the offset effect and can be written as:

$$V = \sqrt{aU_c + b} \tag{6}$$

U_c is the compensated output of the sensor with:

$$U_c = U_s - U_0 + \frac{-b}{a} \tag{7}$$

U_0 is the offset measured during the initialization process before the departure.

Based on this approach, the remaining error would be limited to the non-linearity effect. Illustration of improvements introduced by equation 7 is depicted in figure 5 ('Achieved accuracy with initialization process').

Nonetheless, due to the square root shape of the sensor characteristic, and in spite of improvements achieved with the offset compensation method, the air velocity measurement will remain inaccurate around zero. As shown in figure 5, a few millivolts on sensor output can lead to an error of 0.5 m/s and consequently to an inaccuracy position estimation. In addition, we can also notice that for air velocities higher than 0.6 m/s, the non-linearity effect decreases. Consequently, the sensor becomes less sensitive to the square root for established pedestrian velocities.

D. Offset initialization

As stated before, the accuracy of the anemometer can be improved by the introduction of an offset U_0 to the LBA output voltage U_s. This offset is evaluated by averaging the output during 10 seconds while keeping the velocity equal to zero. From equation (6), U_0 is bounded in order to satisfy that:

$$aU_c + b > 0 \tag{8}$$

According to the shape of the output characteristic (see fig. 3, a is positive. Combining with equation 7, the condition (8) leads to write:

$$U_s > U_0 \tag{9}$$

We have conducted more than 30 trials with measuring the magnitude of $U_s - U_0$ during 10 seconds (with a sampling frequency of 1 kHz) in a static position and formed then the distribution of $U_s - U_0$ (depicted in figure 6). The distribution highlights that for a very low speed, condition ruled by equation (8) is not always observed.

In order to overcome the bias influence, a threshold k is introduced from equation 6 as:

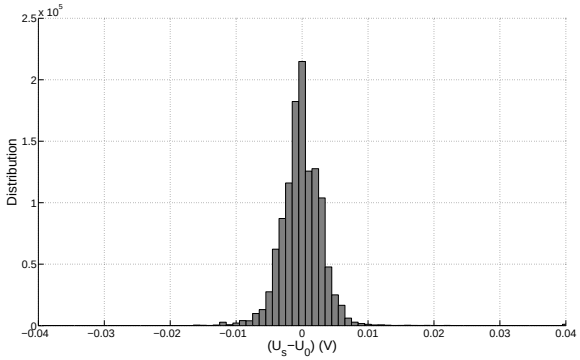

Fig. 6. $U_s - U_0$ distribution of the sensor at zero velocity condition

$$\begin{cases} V = \sqrt{aU_c + b} & U_s > U_0 + k \\ V = 0 & otherwise \end{cases} \tag{10}$$

The threshold k has to be carefully determined in order to keep the sensor sensitive around 0 m/s and to satisfy the condition issued from equation (8). From observations we made from experiments and trials, the threshold k can be determined experimentally. We observed that the distribution $U_s - U_0$ for the zero velocity case and during the walking phase are significantly different. In fact, figure 7 depicts the distribution for the zero velocity case and for large amount of trajectories (7 m, 14 m, 21 m, 28 m, 35 m, 42 m and 49 m). The difference on the shape distribution suggests that the threshold k can be tuned manually with respect to the condition issued from equation (8) and the sensor sensitivity.

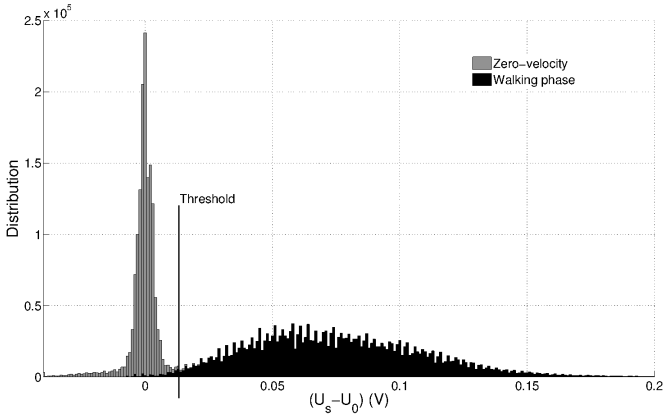

Fig. 7. $U_s - U_0$ distribution for the zero velocity case and for large amount of trajectories

E. Sensor calibration correction for the walking phase

The calibration process involved in III-A has been performed in a wind tunnel with controlled environment conditions. If we achieve the conversion from output voltage to speed rigorously following the calibration process, it appears that an important bias is produced during the walking phase. The bias origin may be explained by the fact that air flow

measurements in a wind tunnel is achieved with constrained flow conditions whereas indoor measurements involve an open atmosphere.

In order to quantify the bias contribution, we have numerically computed an average speed ($\bar{V}$) along different straight paths (7 m, 14 m, 21 m, 28 m, 35 m, 42 m and 49 m). For each path, we repeated the experiment 30 times. Knowing the total elapsed time during the travelled path and the distance, we computed the "true" average speed for each path ($\bar{V}_{true}$). Finally, we formed the error on speed V_{error} for each path and trials as:

$$V_{error} = \bar{V} - \bar{V}_{true} \tag{11}$$

Figure 8 presents the distribution of V_{error} without any correction. It is worth of noting that the average error is around $-1m/s$.

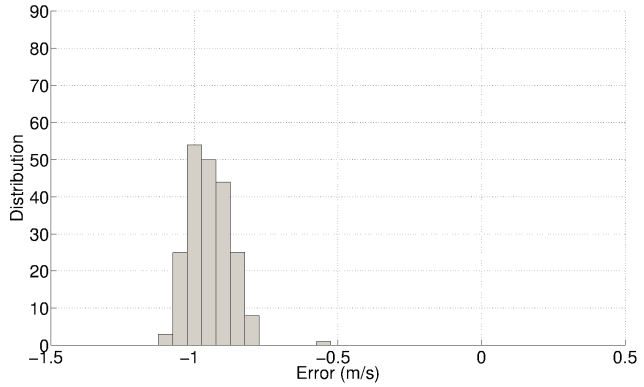

Fig. 8. V_{error} distribution on averaged velocities

Considering the Gaussian shape of the distribution depicted in figure 8, we could assume that V_{error} is following a normal law. Consequently, we can consider V_{error} as the sum of a constant bias b_v and a noise n_v following a normal law as following:

$$V_{error} = b_v + n_v \quad n_v \sim N(0, \sigma_v) \tag{12}$$

Substituting equation (12) into equation 11 leads to write:

$$\bar{V}_{true} = \bar{V} - (b_v + n_v) \tag{13}$$

We aim to correct the characteristic equation 10 which rules the behavior of the sensor in order to bring b_v to 0 and reducing σ_v to minimum. Therefore, we propose to upgrade this equation by adding two correction parameters c_1 and c_2 in order to shift the mean V_{error} distribution from -1 m/s to 0 m/s. Of course, different techniques can be envisaged in order to balance the bias contribution (numerical techniques, recursive approach, sensitivity functions ...). The correction approach we adopted is motivated by its inexpensive computationally feature allowing parameters to be tuned in a on-line way. Therefore, equation 10 is adjusted as following:

$$\begin{cases} V = c_1\sqrt{aU_c + b} + c_2 & U_s > c_1(U_0 + k) + c_2 \\ V = 0 & otherwise \end{cases} \tag{14}$$

We have investigated experimentally the influence of the parameters c_1 and c_2 on the V_{error} distribution shifting. Optimal values of c_1 and c_2 bringing V_{error} distribution from -1 m/s to 0 m/s are respectively 1.4 and 0.75. Figure 9 shows the efficiency of the correction performed on the V_{error} distribution for different straight paths (from 7 m to 49 m).

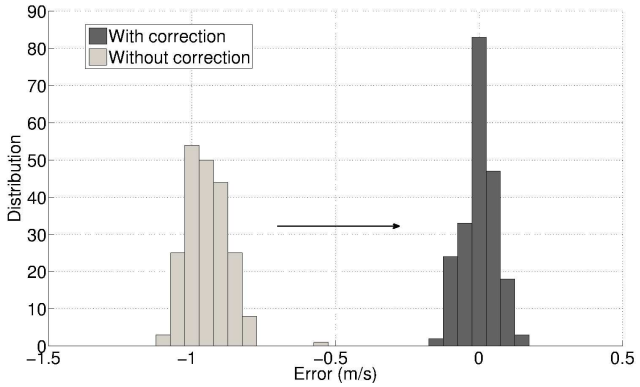

Fig. 9. Shifting of the mean V_{error} distribution from -1 m/s to 0 m/s

IV. PROTOTYPE DESIGN AND EXPERIMENTS

A. Prototype design

Based on previous considerations (see III), first experiments of such sensor revealed the quality of the LBA output signal in terms of reduced noise, fast dynamic response, and appropriate accuracy for the pedestrian context. As mentioned in I, we aim to develop a nomadic compact solution (smartphone oriented solution) based on anemometry sensor integration with the smartphone. Since it is assumed that the sensor will always be oriented in the moving direction (Figure 10), the dynamic pressure is measured in the air flow direction. The static pressure is approximated to the pressure inside the prototype. The display unit of the prototype is provided by the Android device. Sensor data acquisition is performed thanks to a dedicated Microchip PIC 32 bits microcontroller connected to the smartphone via the USB. In addition, numerical computation for position estimation is achieved by the 32 Bits microcontroller (figure 11) in order to avoid risk of interruption due to Android tasks.

Fig. 10. An overview of the device orientation according to the measurement direction

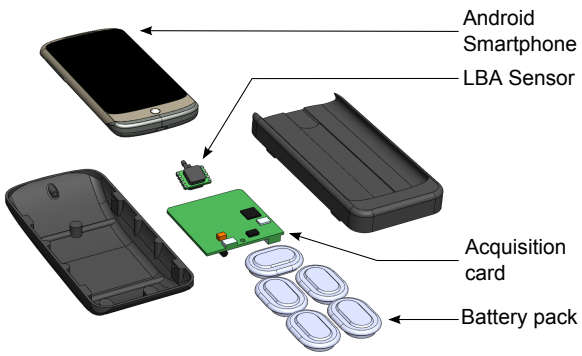

Fig. 11. Detailed view of the main parts of our prototype

B. Experimental protocol

The proposed prototype was tested in a straight corridor for different distance paths of 7 m, 14 m, 21 m, 28 m, 35 m, 42 m and 49 m. For each test, the pedestrian waited 10 seconds before departure to perform the initialization step described in III-C and then start walking along the path with a random speed. This experiment has been done at different hours of the day, first keeping windows closed, without crossing or following people along the path and then without any precautions to study the effect of the draught.

C. Preliminary results and repeatability

The following results are based on 210 measurements recorded at different velocities with the same user and without draught. Figure 12 shows an example of measurements done for a 49 m path. Figure 12(a) illustrates the sensor output U_s, figure 12(b) shows the velocity estimation from equation 14 and figure 12(c) presents the walked distance issued from the numerical integration. It appears that a reduced signal-to-noise ratio is delivered by the sensor and the position according to time is relatively linear (no disturbances affected the velocity measurements).

For the repeatability study, we consider the final pedestrian position during the experiments. Figure 13 shows the obtained position for each length of paths and for the 30 trials for each path. One can note that even if the standard deviation on the speed error is small, its effect on the computed position is growing rapidly. The dispersion of the measured position is indeed of 3 m for a 49 m path. We have noticed that the ratio between the distribution and travelled distance remains bounded to 6 %. The origin of the growing error as the travelled distance increases can be attributed to the constrained correction method (c_1 and c_2 parameters) adopted which could suffer from lack of a robustness to a changing environment. Even if it could appear not accurate, those results are still encouraging for an infrastructure-less indoor localisation approach based on augmented smartphone solution. Improvements are introduced in the conclusion section in order to reduce and limit the effect of the drift.

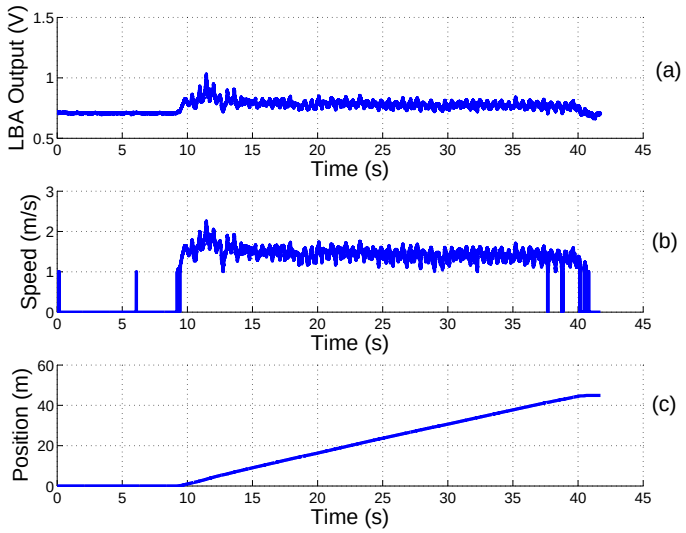

Fig. 12. Example of a 49 m distance path. (a) Anemometer sensor output, (b) velocity estimation and (c) user position from numerical integration.

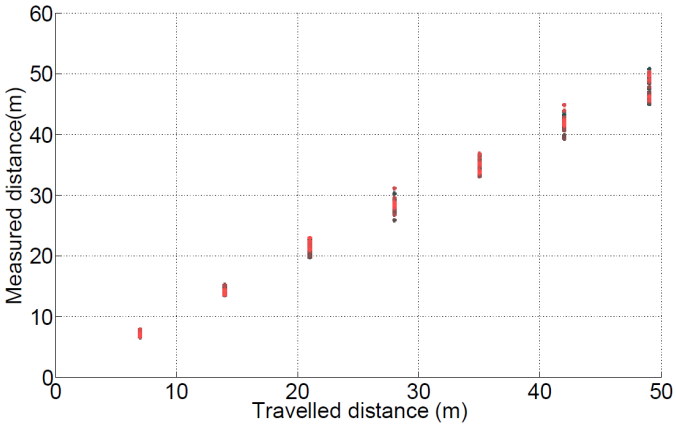

Fig. 13. Repeatability study for different distance paths

D. Draught and air turbulence effects

As the anemometer sensor is based on a linear differential pressure principle, air turbulence may reduce the position

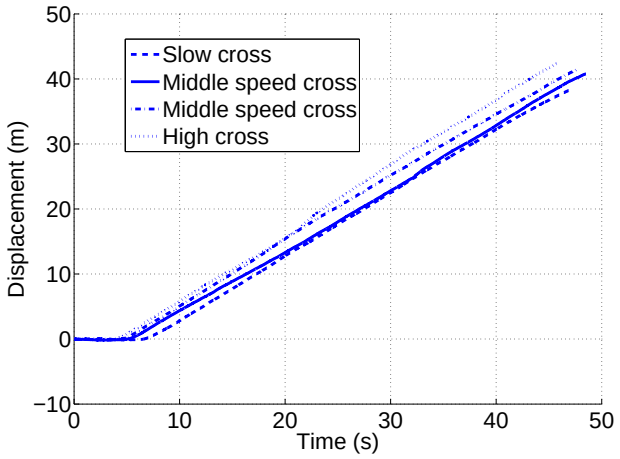

Fig. 14. Influence of turbulence on the position accuracy

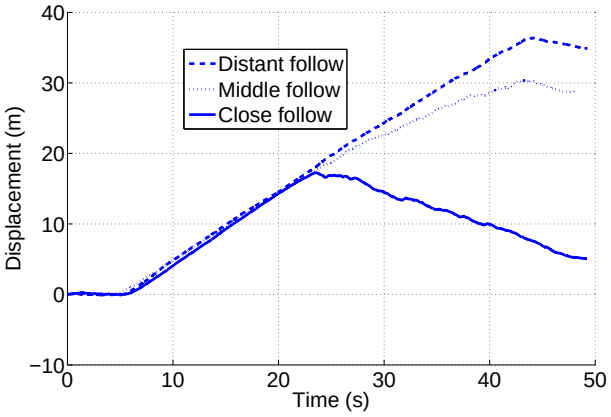

Fig. 15. Influence of a constant air flow on the position estimation

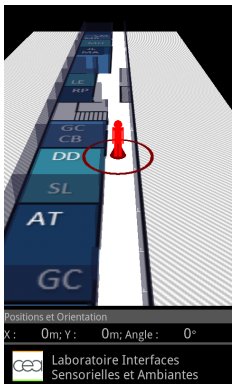

Fig. 16. Overview of the Android display

accuracy. In our case, air turbulence origin can be classified mainly into two category of air streams; turbulence due to passing close to another pedestrian, to an opening door... and established air streams, as draught and building ventilation. In order to quantify the air stream effects on the sensor accuracy, we have conducted experiments involving a pedestrian walking along the 42 m long path at a constant speed and crossed by another pedestrian at a specific location position. This experiment was repeated four times with different crossing speed (from 0.5 m/s to a natural human run). The key issue in the air stream turbulence is the time of exposure of the sensor to the stream. In fact, during the crossing phase, even if it's close, the time of crossing will be short. Therefore, the velocity measurement will be biased for a short time. Numerical integration is involved in the position estimation process. Since the integral calculus has an averaging effect, the impact on the accuracy is minimized. Figure 14 shows different results of crossing phase. We can note that final position error stay in the same range as the previous experiments (see in IV-C).

In case of a constant draught, a constant bias is added to the velocity measurement. Since the bias has not been taken into account in the sensor characteristic, the final position is affected. In order to quantify the magnitude of this effect, we repeated the experiment of the 35 m trajectory following a pedestrian. Different tests, more or less close to the pedestrian (from 50 cm to 2 m), were conducted. Figure 15 shows that a short distance (50 cm) between pedestrians leads to a strong inaccuracy.

E. Android display

In order to offer a complete localisation solution, we have developed an user interface with Android features. The position of the user is displayed during the navigation in the environment (see figure 16).

As stated previously, the anemometer achieves velocity measurements along the walking direction. Moreover, validation experiments have been conducted according to straight paths. To enhance the system's capabilities to planar localisation, a dual-axis gyroscope (IDG300 from InvenSens) is interfaced with the PIC 32 microcontroller for measuring the pedestrian orientation (heading). The position of the user is then calculated according to both sensors signals. Furthermore, the dead reckoning algorithm is update with regards to the gyroscopic measurements. Figure 17 presents an overview of the developed system.

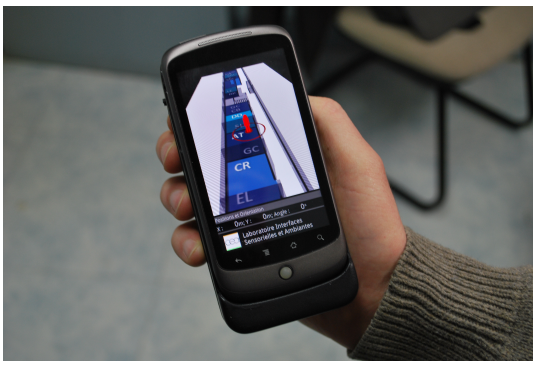

Fig. 17. Overview of the sensor augmented smartphone

V. CONCLUSION

We report in this paper the design of a new sensor coupled with a smartphone dedicated to the indoor localisation issues. The key feature of the system is to achieve the localisation by the combination of compact and low cost sensors (anemometer and gyroscope). Another potential advantage offered by this combination is to achieve indoor pedestrian localisation without the need of deployed infrastructure in the environment. Finally, the device design is oriented towards mobility application by the integration of both localisation and navigation features in the smartphone. Calibration and characterization experiments have been conducted in order to evaluate the added value of the pressure-based anemometer technique. From the first results, the anemometry technique is adapted for performing the pedestrian localisation based on the velocity measurement with regards to some precautions. Therefore, localisation can be achieved with a standard deviation with average accuracy of less than 6 % of the total travelled distance in optimal conditions. However, since the velocity measurement technique relies to the air flow measurement, the sensor is sensitive to environment turbulences. In particular, experiments conducted show the important sensor inaccuracies that can be reached leading to an underestimation of the pedestrian localisation. Even if the performed calibration and biases correction improved significantly the overall accuracy of the sensor, environment changes (temperature, draught ...) induce variabilities in the sensor accuracy. More specifically, the correction method adopted (c_1 and c_2 parameters) has shown a lack in robustness to a changing environment.

Although performances of the device are encouraging, challenges still need to be addressed in the near future. In particular, it remains difficult to obtain repeatable results mainly due to air turbulences. Significant efforts will be put on the air turbulence characterization in order to overcome inaccuracies produced by this technique. Likewise, improvements on the position calculation method is envisaged in order to take into account the encountered situation and tuning the parameters (eg. a, b, c_1, c_2 and k) involved in the position estimation with real-time capabilities. In fact, future works will have to focus on possible improvements with modern filtering solutions. The sensor accuracy should also be improved by the introduction of a map-matching technique allowing the adjustment of the user position according to map excluding unrealistic positions and paths (eg. walking through a wall). Furthermore, a focus will be put on the accuracy determination during the pedestrian navigation. This parameter can be delivered to the user in order to evaluate the confidence ratio to give to the position estimation. Finally, improvements in the user interface will be addressed including features as path planning, point of interest finding and LBS services.

REFERENCES

[1] M. Bshara, U. Orguner, F. Gustafsson, and L. Van Biesen, "Robust tracking in cellular networks using hmm filters and cell-id measurements," *Vehicular Technology, IEEE Transactions on*, vol. 60, no. 3, pp. 1016–1024, 2011.

[2] S. Gezici, Z. Tian, V. Giannakis, H. Kobaysahi, F. Molisch, H. Poor, and Z. Sahinoglu, "Localization via ultra-wideband radios: A look at positioning aspects for future sensor networks," *IEEE trans. Signal Process. Mag.*, vol. 22, no. 4, pp. 70–84, 2005.

[3] S. Holm, "Hybrid ultrasound-rfid indoor positioning: Combining the best of both worlds," in *Proc. IEEE Int RFID Conf*, 2009, pp. 155–162.

[4] H. Liu, H. Darabi, P. Banerjee, and J. Liu, "Survey of wirless indoor positioning techniques and systems," *IEEE trans. On Systems, Man and Cybernetics*, vol. 37, no. 6, pp. 1067–1079, 2007.

[5] D. Skournetou and E. Lohan, "Pulse shaping investigation for the applicability of future gnss signals in indoor environments," in *International Conference on Indoor Positioning and Indoor Navigation (IPIN)*, September 18, 2010.

[6] R. Mautz, "Overview of current indoor positioning systems," *Geodesy and Cartography*, vol. 35, no. 1, pp. 18–22, 2009.

[7] N. Samama, *Global positioning: technologies and performance*, ser. Wiley survival guides in engineering and science. Wiley-Interscience, 2008.

[8] X. Li, J. Wang, A. Olesk, N. Knight, and W. D., "Indoor positioning within a single camera and 3d maps," in *Ubiquitous Positioning Indoor Navigation and Location Based Service (UPINLBS), 2010*, oct. 2010, pp. 1–9.

[9] W. Storms, J. Shockley, and J. Raquet, "Magnetic field navigation in an indoor environment," in *Proc. Ubiquitous Positioning Indoor Navigation and Location Based Service (UPINLBS)*, 2010, pp. 1–10.

[10] E. Foxlin, "Pedestrian tracking with shoe-mounted inertial sensors," *IEEE Comput. Graph. Appl.*, vol. 25, no. 6, pp. 38–46, 2005.

[11] L. Ojeda and J. Borenstein, "Non-gps navigation with the personal dead-reckoning system," in *SPIE Defense and Security Conference, Unmanned Systems Technology IX*, April 9-13 2007.

[12] K. Abdulrahim, C. Hide, T. Moore, and C. Hill, "Aiding mems imu with building heading for indoor pedestrian navigation," in *Proc. Ubiquitous Positioning Indoor Navigation and Location Based Service (UPINLBS)*, 2010, pp. 1–6.

[13] C. Ascher, C. Kessler, M. Wankerl, and G. F. Trommer, "Dual imu indoor navigation with particle filter based map-matching on a smartphone," in *Proc. Int Indoor Positioning and Indoor Navigation (IPIN) Conf*, 2010, pp. 1–5.

[14] M. El-Diasty and S. Pagiatakis, "Calibration and stochastic modelling of inertial navigation sensor errors," *JGPS*, vol. 7, pp. 170–182, 2008.

[15] ——, "A rigorous temperature-dependent stochastic modelling and testing for mems-based inertial sensor errors," *Sensors*, vol. 9, pp. 8473–8489, 2009.

[16] S. Lamy-Perbal, M. Boukallel, and N. Castaneda, "An improved pedestrian inertial navigation system for indoor environments," in *Proc. IEEE/RSJ Int Intelligent Robots and Systems (IROS) Conf*, 2011, pp. 2505–2510.

[17] T. Robin, G. Antonini, M. Bierlaire, and J. Cruz, "Specification, estimation and validation of a pedestrian walking behavior model," *Transportation Research Part B: Methodological*, vol. 43, no. 1, pp. 36 – 56, 2009.